Sciencexpress Research Articles

Observation of Majorana fermions in ferromagnetic atomic chains on a superconductor

Stevan Nadj-Perge,[1]* Ilya K. Drozdov,[1]* Jian Li,[1]* Hua Chen,[2]* Sangjun Jeon,[1] Jungpil Seo,[1] Allan H. MacDonald,[2] B. Andrei Bernevig,[1] Ali Yazdani[1]†

[1]Joseph Henry Laboratories and Department of Physics, Princeton University, Princeton, NJ 08544, USA.
[2]Department of Physics, University of Texas at Austin, Austin, TX 78712, USA.

*These authors contributed equally to this work.

†Corresponding author. E-mail: yazdani@princeton.edu

Majorana fermions are predicted to localize at the edge of a topological superconductor, a state of matter that can form when a ferromagnetic system is placed in proximity to a conventional superconductor with strong spin-orbit interaction. With the goal of realizing a one-dimensional topological superconductor, we have fabricated ferromagnetic iron (Fe) atomic chains on the surface of superconducting lead (Pb). Using high-resolution spectroscopic imaging techniques, we show that the onset of superconductivity, which gaps the electronic density of states in the bulk of the Fe chains, is accompanied by the appearance of zero energy end states. This spatially resolved signature provides strong evidence, corroborated by other observations, for the formation of a topological phase and edge-bound Majorana fermions in our atomic chains.

Topological superconductors are a distinct form of matter that is predicted to host boundary Majorana fermions (*1–3*). These quasi-particles are the emergent condensed matter analogs of the putative elementary spin-1/2 particles originally proposed by Ettore Majorana (*4*) with the intriguing property of being their own anti-particles. Super-symmetric theories in particle physics and some models for dark matter in cosmology motivate an ongoing search for free Majorana particles (*5*, *6*). The search for Majorana quasi-particle (MQP) bound states in condensed matter systems is motivated in part by their potential use as topological qubits to perform fault-tolerant computation aided by their non-Abelian characteristics (*7*, *8*). Spatially separated pairs of MQP pairs can be used to encode information in a nonlocal fashion, making them more immune to quantum decoherence. Early proposals for the detection of MQPs were based on the properties of superfluid ^{3}He, on exotic fractional quantum Hall states, or on correlated superconductors (*9–12*). The focus in the last few years has shifted to the search for these exotic fermions in weakly interacting synthetic systems in which proximity to a conventional Bardeen-Cooper-Schrieffer (BCS) superconductor is used in concert with other electronic properties to create the topological phase that hosts MQPs.

The idea that MQPs can be engineered in the laboratory grew from the theoretical observation that proximity induced superconductivity on the surface state of a topological insulator is topological in nature (*13*). Pairing on a "spin-less" Fermi surface (*1*), created in this case by the spin-momentum locking of topological surface states, must be effectively p-wave to satisfy the pair-wavefunction anti-symmetry requirement and is therefore topological. This approach was later extended to systems in which a semiconductor nanowire with strong spin orbit interactions in a parallel magnetic field is in contact with a superconductor (*14*, *15*). Experimental efforts to implement the nanowire proposal have uncovered evidence for a zero bias peak (ZBP) in tunneling spectroscopy studies of hybrid superconductor-semiconductor nanowire devices, as expected in the presence of the MQP states of a topological superconductor (*16–19*). However, the ZBPs detected in such devices could also be caused by the Kondo effect or disorder (*20–24*). A key disadvantage of the nanowire studies is that they lack the ability to spatially resolve ZBP features in order to demonstrate that they are localized at the boundary of a gapped superconducting phase. Here we introduce a method of fabricating one-dimensional topological superconductors and detecting their MQPs that achieves both spatial and spectral resolution.

Magnetic atomic chains as a platform for topological superconductivity

Magnetic atom chains on the surface of a conventional s-wave superconductor have been proposed to provide a versatile platform for the realization of topological superconductors (*25*). This platform lends itself to the detection of MQPs using the spectroscopic imaging techniques of scanning tunneling microscopy (STM). In the absence of intrinsic spin-orbit coupling, (*25*) and related theoretical work (*26–30*) showed that a topological phase emerges in an atomic chain when its magnetic atoms have a spatially modulated spin arrangement, for example a spin helix. The spin texture of the chains emulates the combination of spin-orbit and Zeeman interactions required to create a topological phase. Helical spin configurations are however much less common in atomic chains than simple ferromagnetic and antiferromagnetic ones or may be more influenced by disorder (*31*). We therefore explore an alternate, more realizable scenario by placing a Fe chain on the surface of Pb (Fig. 1A). We will show that the essential ingredients for topological superconductivity in this scenario are the ferromagnetic interaction between Fe atoms realized at the Fe-Fe bond distance and the strong spin-orbit interaction in superconducting Pb (*32*). Our approach is related to earlier proposals for topological superconductivity using half-metal ferromagnets or metallic chains placed in contact with superconductors in the presence of spin-orbit interactions (*33–35*).

To illustrate the key ingredient of our approach, we first consider an idealized ferromagnetic chain of Fe atoms described by a tight-binding model calculation [section 1 of (*36*)]. We use hopping parameters appropriate for d orbitals of bulk Fe to compute the band structure of a freely suspended linear Fe chain (Fig. 1B). The large exchange interaction results in a fully occupied majority spin band with the Fermi level (E_F) residing in the minority spin bands. Coupling the Fe chain to a BCS superconductor with strong spin-orbit interaction (such as Pb), we find that the spin-orbit interactions lift many of the degeneracies in the chain's band structure shown in Fig. 1B, while at the same time allowing for the occurrence of p-wave superconductivity [section 1 of (*36*)]. Since only the Fe *d*-bands will be strongly spin-polarized, other bands are unlikely to influence the topological character of the system, whether they reside mainly on the Fe chains or on the substrate. Remarkably, for large exchange interaction, topological superconductivity is ubiquitous to the type of band structure shown in Fig. 1B—occurring for nearly all values of the chemical potential [Fig. 1C and (*36*) for details]. In this idealized situation, the number of minority spin bands which cross the Fermi level is almost always odd, making the presence of MQPs at the ends of the

Downloaded from http://science.sciencemag.org/ on October 25, 2017

chains almost guaranteed.

We consider another idealized situation for topological superconductivity by modeling a ferromagnetic chain embedded in a 2D superconductor, which allows us identify its signatures in STM measurements [section 2 of (*36*)]. The spatially resolved density of states (DOS) of this 2D model at positions on the chain differs from that of a BCS superconductor by the presence of Yu-Shiba-Rusinov in-gap states (Fig. 1, C and D) (*37–41*). These calculations also exhibit the spatial and spectroscopic signatures of MQPs at the chain ends (Fig. 1, D and E). Other more realistic models for our experimental system are also worth exploring (see below) and non-topological phases can occur for some chain geometries. These model studies of proximity-induced superconductivity on Fe chains demonstrate that topological states can be identified using STM by establishing: 1) ferromagnetism on the chain, 2) spin-orbit coupling in the host superconductor (or at its surface), 3) a superconducting gap in the bulk of the chain, and finally 4) a localized ZBP due to MQPs at the ends of the chain. One can over constrain these conditions by providing evidence that the system has an odd number of band crossings at E_F. The disappearance of edge-localized ZBPs when the underlying superconductivity is suppressed provides an additional check to show that the MQP signature is associated with superconductivity and not with other phenomena, such as the Kondo effect (*20–22*).

Ferromagnetic Fe atomic chains on the Pb(110) surface

To fabricate an atomic chain system on the surface of a superconductor with strong spin-orbit coupling, we used a Pb (110) single crystal, which we prepare with cycles of in situ sputtering and annealing. Following sub-monolayer evaporation of Fe on the Pb surface at room temperature and light annealing, STM images (temperature was 1.4K for all experiments reported here) show large atomically ordered regions of the Pb (110) surface, as well as islands and chains of Fe atoms that have nucleated on the surface (Fig. 2A). The islands appear to provide the seed from which chains self-assemble following the anisotropic structure of the underlying surface. Depending on growth conditions, we find Fe chains as long as 500 Å, usually with an Fe island in the middle (inset, Fig. 2A). In longer chains, the ends are separated from the islands in the middle by atomically ordered regions that are 200 Å long. High-resolution STM images show that the chains (with an apparent height of about 2 Å) are centered between the atomic rows of Pb (110), display weak atomic corrugation (5-10 pm) and strain the underlying substrate (Fig. 2, B to D). Approximate periodicities of 4.2Å and 21Å measured on the chain show that the Fe chain has a structure that is incommensurate with that of the underlying Pb surface. To identify the atomic structure of our chains, we performed density functional theory (DFT) calculations of Fe on the Pb (110) surface which show that strong Fe-Pb bonding results in a partially submerged zigzag chain of Fe atoms between Pb (110) atom rows [Fig. 2, E and F; see section 3 of (*36*) for DFT details]. From these calculations, we find that among several candidate structures with the experimental periodicity, a three-layer Fe zigzag chain partially submerged in Pb has the lowest energy and gives contours of constant electron density most consistent with our STM images.

We use a combination of spectroscopic and spin-polarized measurements to demonstrate that Fe atomic chains on Pb (110) satisfy the criteria (conditions 1-4 above) required to demonstrate a one-dimensional topological superconductor. First, we discuss spin-polarized STM studies that show experimental evidence for ferromagnetism on the Fe chains and strong spin-orbit coupling on the Pb surface (Fig. 3, A to C). Using Cr STM tips, which have been prepared using controlled indentation of the tip into Fe islands, we measured tunneling conductance (dI/dV) at a low bias (V = 30 mV) as a function of magnetic field perpendicular to the surface on both the chains and on the Pb substrate (Fig. 3, A and B). Our preparation of spin-polarized tips were validated by also performing experiments on Co on Cu (111), now a standard system (*40*) for verifying spin-polarized STM capabilities, in situ during the same experimental runs. The spin-polarized measurements on the Fe chains show hysteresis loops characteristic of tunneling between two ferromagnets with the field switching only one of them (at around 0.25 T) (*42*, *43*). The strength of the spin-polarized STM signal varies along the chain, likely due to the electronic and structural properties of our zigzag Fe chains. We find that tunneling with the same tip on the Pb (110) surface far from the Fe chains also shows field-dependent conductance. In contrast to the asymmetric behavior observed on the chains, the field dependence on the substrate is symmetric with field, as expected for tunneling into non-magnetic Pb, but still shows the switching behavior that is due to magnetization reversal of the tip. Similar tunneling magnetoresistance curves have been previously reported for tunneling from a ferromagnet into semiconductors and have been attributed to spin-polarized tunneling in the presence of strong spin-orbit interactions (*44*). The field-dependent signal on Pb is consistent with a preference for spins to be in the plane of the surface, in which case further polarization of the tip's magnetization perpendicular to the surface suppresses tunneling conductance. The size of this signal depends on the orientation of the tip's magnetization relative to that of the spins at the surface. This observation is consistent with a Rashba-like ($k \cdot \sigma$) spin-orbit coupling at the Pb (110) surface upon which our ferromagnetic Fe chain is self-assembled.

Our DFT calculations confirm that the zigzag Fe chains in Pb (110) are likely ferromagnetic [section 3 of (*36*)], as expected given that the distance between the Fe atoms is close to that of bulk Fe. These calculations also demonstrate that Fe chains on Pb have exchange energy J of about 2.4 eV and a magnetic anisotropy energy (1.4 meV/Fe atom) that is large enough to suppress thermal fluctuations in the magnetic configuration. The large anisotropy also implies that very large fields are required to switch the chain's magnetization orientation, consistent with our finding that low fields only reorient the tip's magnetization.

Our model studies demonstrate that topological superconductivity occurs when an odd number of 1D bands cross the Fermi energy. We now focus on obtaining information on the electronic structure of our Fe chains from STM spectroscopy. As shown in Fig. 3D, the Fe chain contribution to the DOS has two distinct peaks separated by about 0.9 eV, one above and the other below E_F. To understand the origin of this double-peak structure, we have carried out a number of model calculations, including those based on tight binding and DFT for our specific zigzag Fe structures identified by comparing DFT to STM images (Fig. 2, C to F). The results of these calculations, for both suspended and Pb-imbedded chains [sections 3 and 4 in (*36*)] indicate that E_F for such a system lies in the Fe minority bands and that the double-peak structure is related to structure-specific features of the minority-band bonding pattern. Moreover, the tight-binding model that reproduces the experimentally observed double-peak structure (Fig. 3E) shows the number of band crossing at E_F to be odd [phase diagram in section 4 in (*36*)]. Although momentum-resolved DOS measurements with the STM will be required to more directly probe the band structure of the chains, the correspondence between model calculations and the measured DOS is very suggestive that the band structure of these chains is consistent with topological superconductivity. All the chains we examined in search for MQPs share the above structural and electronic characteristics.

Superconductivity on Fe atomic chains and signatures of MQP

We use high resolution spectroscopy and spectroscopic mapping, with both normal and superconducting tips, to establish the signature of both the pairing gap on our Fe chains and of the MQP at their ends at low temperatures (1.4 K) (Figs. 4 and 5). In Fig. 4, we show spatially resolved spectra, as well as spectroscopic maps with a normal tip, on both the substrate and the Fe chain. Examining the spectra away from the Fe chain on the Pb surface, we resolved a superconducting gap that can be

Downloaded from http://science.sciencemag.org/ on October 25, 2017

modeled with the thermally broadened (T = 1.4 K) BCS density of states with Pb's bulk pairing gap (Δ_s = 1.36 meV) (Fig. 4A, lowest curve). In the middle of the chains, spatially resolved spectroscopic measurements show the formation of features in the Pb gap, with asymmetric edges at roughly ±1 meV, which evolve to include a sharp ZBP that is prominently detected about 15-20 Å from the ends of the chain. Figure 4, B to E show such ZBPs at two ends of the same chain that grow out of an Fe island. Approaching the island, the spectra on both sides of the chain also show enhanced low-energy DOS, but at these locations, the structure of the chains is not known [example in fig. S14 in (*36*)]. Spectroscopic maps in Fig. 4F visualize the spatial structure of excitations at different energies and clearly show the localized nature of the ZBPs at one end of the chain and the delocalized nature of the excitations at higher energies throughout the chain. These maps also resolve the spatially modulated decay of the ZBP away from the chain ends that is anticipated from model calculations [section 2 of (*36*)]. Our ability to correlate the location of the ZBP with the end of our atomic chains is one of the main experimental requirements for interpreting that this feature is associated with the predicted MQP of a topological superconductor. We have confirmed the robust observation of ZBPs at the end of multiple chains (more than ten), measured with different tips, on different experimental runs with freshly prepared Pb and Fe chains (see section 5 of (*36*) for more examples).

To obtain more precise information about the pairing gap induced on the Fe chains, we have also carried out spectroscopic measurements with superconducting tips, prepared in situ by contacting a W tip with the Pb surface (Fig. 5). Away from the Fe chains, the spectra measured with these tips show the behavior expected for tunneling between two superconductors, with sharp peaks at energies corresponding to the sum of the BCS gaps on the tip Δ_T and the substrate Δ_S (Fig. 5A). The singularity in DOS at the gap edge in this case allows us to resolve finer features within the thermally broadened DOS of our chains. At the end of the chains, spectroscopy with the superconducting tips shows a sharp peak at $|eV| = \Delta_T$ corresponding to the peaks at these locations identified as ZBPs when measured with the normal tips (Fig. 5B). Spectroscopic maps with the superconducting tip at this energy also show this feature to be the most pronounced at the end of the chains (Fig. 5D, middle panel) as expected for bound MQPs. At other locations in the middle (bulk) of the chains (Fig. 5, C and D), this signature of MQPs is greatly suppressed, but there are sharp peaks at higher energies $|eV| > \Delta_T$ that can be attributed to the edge of a pairing gap at about 200-300 μeV. Using a model calculation of scattering of electrons in an Fe chain from a Pb(110) surface, we estimate that the effective Rashba spin-orbit interaction strength induced on the chain by the Pb substrate [section 6 of (*36*)] is about 0.11 eV-Å. Using this value in our simple linear chain calculation of Fig. 1, B and C, yields a value for the p-wave gap of around 100 μeV, which is qualitatively consistent with our experimental results [section 1 of (*36*)]. Separate calculations for an embedded zigzag structure using Pb's bulk atomic spin-orbit coupling also yield a similar value [section 4 of (*36*)]. The qualitative agreement between the theoretical and experimental estimates of p-wave gap is remarkable considering the many uncertainties that we have not taken into account, e.g., surface relaxation, surface dipole, lattice mismatch, and modification of s-wave pair potentials near the surface of Pb. The size of this pairing gap is also consistent with the low-energy background tunneling conductance (50% of the normal state) observed at 1.4 K in the middle of the wire with the normal tip, as shown in Fig. 4 [see also section 9 of (*36*) for more details]. We also note that our experiments are in a regime where coupling strength between the STM tip and the MQP at the end of our chains is small in energy, as compared to the thermal energy, resulting in the suppression of the zero bias conductance (1.3×10^{-4} e^2/h, as shown in Fig. 4) from the ideal value of $2e^2/h$ (*45*). Evidence for a gap in the middle of our chains, with a value that is in line with model calculations, together with ZBPs at their ends completes the list of experimental observations required to conclude that superconductivity on our ferromagnetic atomic chains is topological in nature.

Finally, we comment on the particle-hole asymmetric features at energies above the minimum gap of our chain measured with normal tips (near ±1 meV) throughout the chain, shown in Fig. 4). These features in the spectra are reproducible and reminiscent of the band of Yu-Shiba-Rusinov in-gap states found in the 2D model calculation of Fig. 1D. Our DFT calculations show that there is significant charge transfer from the Pb substrate to the Fe chain, resulting in a linear dipole moment density (per Å) of 0.02 e·Å perpendicular to the Pb surface. As in the case of isolated magnetic impurities, this potential makes tunneling in to and out of the in-gap states asymmetric (see also results of simulations in Fig. 1D that include such a potential) (*40*, *41*). These in-gap states also change approaching the end of our chains; however, they are always distinct in energy from the ZBP we associate with the MQP, even at the end of the chain [see fig. S14 in (*36*) for example].

Experimental checks for interpretations other than MQPs

To address alternatives to the MQP interpretation of the ZBP, we have carried out a number of control experiments. First, we examine the possibility of the ZBP being due to a Kondo resonance, which has been raised in the context of semiconductor nanowire experiments where there is experimental evidence for a Kondo effect (*21*, *22*). To address this issue, we have carried out experiments in weak magnetic fields (0.1T) that suppress superconductivity in the Pb substrate. All features associated with the gap in the middle of the chains and the ZBP at their ends disappear in the absence of superconductivity in Pb [section 7 of (*36*)]. If the ZBPs at the ends of the chains were due to the Kondo effect, we expect that increasing the DOS near E_F in the normal state would only enhance the ZBP rather than suppress it. The importance of superconductivity to the formation of the ZBP also rules out alternative scenarios in which such peaks appear due to disorder effects. Second, our spin-polarized STM measurements do not show significant magnetization change at the end of the chain, which discounts the unlikely scenario in which the pairing gap at the end of the chain is strongly suppressed and therefore gives an apparent ZBP. Third, structural and potential defects in our substrate cannot produce in-gap states (including ZBPs) in accordance with Anderson's theorem and previous experiments, which show that, for conventional s-wave superconductors, in-gap states are not induced by non-magnetic adsorbates or step edges (*40*, *41*).

Finally, we add that we have found very short Fe chains (~30-40 Å) in which the ZBPs are strongly suppressed [section 8 of (*36*)]. This observation suggests that coupling the end states to each other suppresses the signatures we are associating with MQPs. Although more detailed length dependence experiments are needed to characterize the decay length of MQP end states more quantitatively, this experiment establishes that our ZBPs are not associated with disorder at the end of our chains. More specifically, our model calculations show the wavefunction of the MQP at one end of our hybrid chain-superconductor system to have a combination of power-law decay (on the Fermi length scale) and an exponential decay (related to the p-wave pairing's coherence length) as a function of distance from the end of the chains [section 2 of (*36*)] (*46*). Our experimentally observed decay of the ZBP over 15-20 Å (Figs. 4 and 5) is likely associated with the power-law decay and the effective Fermi wavelength in our chain and is consistent with the suppression of the MQP signatures in chains of double that length. The small ZBP splitting that may be present even in our longest chains is smaller than our energy resolution, which is about 100 μeV for measurements with the superconducting tip. Besides the coupling between the MQPs on either side of a chain, there are situations where multiple channels on the chain can give rise to multiple MQP at the same end of the chain [section 2 of (*36*)]. Generically, a perturbation can couple and split these MQPs, un-

Downloaded from http://science.sciencemag.org/ on October 25, 2017

less they are protected by a symmetry [see for example, (*47*)] of the system, resulting in the absence of topological superconductivity. Ultimately, the splitting of our MQPs needs to be experimentally tested using higher-resolution measurements. Our ability to characterize splitting is limited by thermal broadening (1.4 K), which accounts for the width of the experimental features and contributes to the background tunneling conductance at zero bias—so-called quasi-particle poisoning of MQP [section 9 of (*36*)] Future studies will require milli-kelvin STM measurements, a capability that has already been demonstrated in experiments on other exotic superconductors (*48*). Overall, based on the results of these control experiments together with the observation of all 4 enumerated experimental signatures, we conclude that our results are consistent with the realization of a topological superconducting state with localized MQPs.

Outlook

The experimental system described here demonstrates a platform for future experiments to manipulate MQPs and to realize other related one or two-dimensional topological superconducting phases. An obvious extension of our experiments is to 2D islands of ferromagnetic films on the surface of Pb. Provided these films are thin enough, a few monolayer as in our chains, pairing could be stabilized at a reasonable temperature and the edges of these islands could harbor propagating Majorana modes. The detailed structure of such modes, whether they can be chiral or fully in-gap, depends on the spin-orbit coupling configuration. Searching for other systems with both even or odd number of band crossing at E_F on Pb can be used to further test the concept behind our studies and should show both topological and non-topological superconducting phases. Although the phase with the even number of crossing at the E_F is not topological, it is a model system to form the Fulde-Ferrell-Larkin-Ovchinnikov (FFLO) phase that has a modulated gap structure with a periodicity related to (in the simplest case) the difference between the two Fermi points (1D) or circles (2D) (*49*, *50*). STM spectroscopic mapping can be used to characterize the modulated gap structure of this system and provide evidence for an FFLO phase.

Ultimately, manipulation of MQPs is required to demonstrate braiding and the non-Abelian characteristics of these quasi-particles. We have recently proposed that application of a parallel magnetic field to ring like magnetic atomic structures fabricated on a thin film superconductor can be used to generate edges between trivial and topological regions with MQP in such rings (*51*). The rotation of the parallel magnetic field (that does not perturb superconductivity in thin films) can then be used to manipulate and braid MQPs in ring like atomic structures. This proposal applies to both the spin-helix arrangement of magnetism as well as to the ferromagnetic chains studied here. In addition to manipulating MQPs, parallel field applied to a chain on a thin film superconductor can also be used to drive the chains between topological and trivial superconducting phases. Ultimately, atomic manipulation techniques with the STM can be used to fabricate complex magnetic structures in which MQP may be engineered and manipulated.

References and Notes

1. A. Y. Kitaev, Unpaired Majorana fermions in quantum wires. *Physics-Uspekhi* **44**, 131–136 (2001). doi:10.1070/1063-7869/44/10S/S29
2. J. Alicea, New directions in the pursuit of Majorana fermions in solid state systems. *Rep. Prog. Phys.* **75**, 076501 (2012). Medline doi:10.1088/0034-4885/75/7/076501
3. C. W. J. Beenakker, Search for Majorana fermions in superconductors. *Annu. Rev. Condens. Matter Phys.* **4**, 113–136 (2013). doi:10.1146/annurev-conmatphys-030212-184337
4. E. Majorana, Teoria simmetrica dell'elettrone e del positrone. *Nuovo Cim.* **14**, 171–184 (1937). doi:10.1007/BF02961314
5. F. Wilczek, Majorana returns. *Nat. Phys.* **5**, 614–618 (2009). doi:10.1038/nphys1380
6. D. Wark, Particle physics: The hunt for Majorana neutrinos hots up. *Nature* **510**, 224–225 (2014). Medline doi:10.1038/nature13501
7. A. Y. Kitaev, Fault-tolerant quantum computation by anyons. *Ann. Phys.* **303**, 2–30 (2003). doi:10.1016/S0003-4916(02)00018-0
8. C. Nayak, S. H. Simon, A. Stern, M. Freedman, S. Das Sarma, Non-Abelian anyons and topological quantum computation. *Rev. Mod. Phys.* **80**, 1083–1159 (2008). doi:10.1103/RevModPhys.80.1083
9. M. M. Salomaa, G. E. Volovik, Cosmiclike domain walls in superfluid ^3B: Instantons and diabolical points in (*k*,*r*) space. *Phys. Rev. B* **37**, 9298–9311 (1988). doi:10.1103/PhysRevB.37.9298
10. G. Moore, N. Read, Nonabelions in the fractional quantum Hall effect. *Nucl. Phys. B* **360**, 362–396 (1991). doi:10.1016/0550-3213(91)90407-O
11. N. Read, D. Green, Paired states of fermions in two dimensions with breaking of parity and time-reversal symmetries and the fractional quantum Hall effect. *Phys. Rev. B* **61**, 10267–10297 (2000). doi:10.1103/PhysRevB.61.10267
12. D. A. Ivanov, Non-Abelian statistics of half-quantum vortices in p-wave superconductors. *Phys. Rev. Lett.* **86**, 268–271 (2001). Medline doi:10.1103/PhysRevLett.86.268
13. L. Fu, C. L. Kane, Superconducting proximity effect and majorana fermions at the surface of a topological insulator. *Phys. Rev. Lett.* **100**, 096407 (2008). Medline doi:10.1103/PhysRevLett.100.096407
14. R. M. Lutchyn, J. D. Sau, S. Das Sarma, Majorana fermions and a topological phase transition in semiconductor-superconductor heterostructures. *Phys. Rev. Lett.* **105**, 077001 (2010). Medline doi:10.1103/PhysRevLett.105.077001
15. Y. Oreg, G. Refael, F. von Oppen, Helical liquids and Majorana bound states in quantum wires. *Phys. Rev. Lett.* **105**, 177002 (2010). Medline doi:10.1103/PhysRevLett.105.177002
16. V. Mourik, K. Zuo, S. M. Frolov, S. R. Plissard, E. P. Bakkers, L. P. Kouwenhoven, Signatures of Majorana fermions in hybrid superconductor-semiconductor nanowire devices. *Science* **336**, 1003–1007 (2012). Medline doi:10.1126/science.1222360
17. A. Das, Y. Ronen, Y. Most, Y. Oreg, M. Heiblum, H. Shtrikman, Zero-bias peaks and splitting in an Al–InAs nanowire topological superconductor as a signature of Majorana fermions. *Nat. Phys.* **8**, 887–895 (2012). doi:10.1038/nphys2479
18. M. T. Deng, C. L. Yu, G. Y. Huang, M. Larsson, P. Caroff, H. Q. Xu, Anomalous zero-bias conductance peak in a Nb-InSb nanowire-Nb hybrid device. *Nano Lett.* **12**, 6414–6419 (2012). Medline doi:10.1021/nl303758w
19. A. D. K. Finck, D. J. Van Harlingen, P. K. Mohseni, K. Jung, X. Li, Anomalous modulation of a zero-bias peak in a hybrid nanowire-superconductor device. *Phys. Rev. Lett.* **110**, 126406 (2013). Medline doi:10.1103/PhysRevLett.110.126406
20. J. Liu, A. C. Potter, K. T. Law, P. A. Lee, Zero-bias peaks in the tunneling conductance of spin-orbit-coupled superconducting wires with and without Majorana end-states. *Phys. Rev. Lett.* **109**, 267002 (2012). Medline doi:10.1103/PhysRevLett.109.267002
21. E. J. H. Lee, X. Jiang, R. Aguado, G. Katsaros, C. M. Lieber, S. De Franceschi, Zero-bias anomaly in a nanowire quantum dot coupled to superconductors. *Phys. Rev. Lett.* **109**, 186802 (2012). Medline doi:10.1103/PhysRevLett.109.186802
22. H. O. H. Churchill, V. Fatemi, K. Grove-Rasmussen, M. T. Deng, P. Caroff, H. Q. Xu, C. M. Marcus, Superconductor-nanowire devices from tunneling to the multichannel regime: Zero-bias oscillations and magnetoconductance crossover. *Phys. Rev. B* **87**, 241401 (2013). doi:10.1103/PhysRevB.87.241401
23. D. I. Pikulin, J. P. Dahlhaus, M. Wimmer, H. Schomerus, C. W. J. Beenakker, A zero-voltage conductance peak from weak antilocalization in a Majorana nanowire. *New J. Phys.* **14**, 125011 (2012). doi:10.1088/1367-2630/14/12/125011
24. G. Kells, D. Meidan, P. W. Brouwer, Near-zero-energy end states in topologically trivial spin-orbit coupled superconducting nanowires with a smooth confinement. *Phys. Rev. B* **86**, 100503 (2012). doi:10.1103/PhysRevB.86.100503
25. S. Nadj-Perge, I. K. Drozdov, B. A. Bernevig, A. Yazdani, Proposal for realizing Majorana fermions in chains of magnetic atoms on a superconductor. *Phys. Rev. B* **88**, 020407 (2013). doi:10.1103/PhysRevB.88.020407
26. F. Pientka, L. I. Glazman, F. von Oppen, Topological superconducting phase in helical Shiba chains. *Phys. Rev. B* **88**, 155420 (2013). doi:10.1103/PhysRevB.88.155420

Downloaded from http://science.sciencemag.org/ on October 25, 2017

27. J. Klinovaja, P. Stano, A. Yazdani, D. Loss, Topological superconductivity and Majorana fermions in RKKY systems. *Phys. Rev. Lett.* **111**, 186805 (2013). Medline doi:10.1103/PhysRevLett.111.186805
28. B. Braunecker, P. Simon, Interplay between classical magnetic moments and superconductivity in quantum one-dimensional conductors: Toward a self-sustained topological Majorana phase. *Phys. Rev. Lett.* **111**, 147202 (2013). Medline doi:10.1103/PhysRevLett.111.147202
29. M. M. Vazifeh, M. Franz, Self-organized topological state with Majorana fermions. *Phys. Rev. Lett.* **111**, 206802 (2013). Medline doi:10.1103/PhysRevLett.111.206802
30. S. Nakosai, Y. Tanaka, N. Nagaosa, Two-dimensional p-wave superconducting states with magnetic moments on a conventional s-wave superconductor. *Phys. Rev. B* **88**, 180503 (2013). doi:10.1103/PhysRevB.88.180503
31. Y. Kim, M. Cheng, B. Bauer, R. M. Lutchyn, S. Das Sarma, Helical order in one-dimensional magnetic atom chains and possible emergence of Majorana bound states. *Phys. Rev. B* **90**, 060401(R) (2014). doi:10.1103/PhysRevB.90.060401
32. A. Yazdani, "Visualizing topological quantum states: From Dirac to Majorana fermions," presentation at Nobel Symposium on "New Forms of Matter," Högberga Gård, Lidingö, Sweden, 13 to 15 June 2014.
33. M. Duckheim, P. W. Brouwer, Andreev reflection from noncentrosymmetric superconductors and Majorana bound-state generation in half-metallic ferromagnets. *Phys. Rev. B* **83**, 054513 (2011). doi:10.1103/PhysRevB.83.054513
34. S. B. Chung, H. J. Zhang, X. L. Qi, S. C. Zhang, Topological superconducting phase and Majorana fermions in half-metal/superconductor heterostructures. *Phys. Rev. B* **84**, 060510(R) (2011). doi:10.1103/PhysRevB.84.060510
35. A. C. Potter, P. A. Lee, Topological superconductivity and Majorana fermions in metallic surface states. *Phys. Rev. B* **85**, 094516 (2012). doi:10.1103/PhysRevB.85.094516
36. Materials and methods are available as supplementary materials on *Science* Online.
37. L. Yu, *Acta Phys. Sin.* **21**, 75 (1965).
38. H. Shiba, Classical spins in superconductors. *Prog. Theor. Phys.* **40**, 435–451 (1968). doi:10.1143/PTP.40.435
39. A. I. Rusinov, *Sov. Phys. JETP* **9**, 85 (1969).
40. A. Yazdani, B. A. Jones, C. P. Lutz, M. F. Crommie, D. M. Eigler, Probing the local effects of magnetic impurities on superconductivity. *Science* **275**, 1767–1770 (1997). Medline doi:10.1126/science.275.5307.1767
41. A. Balatsky, I. Vekhter, J.-X. Zhu, Impurity-induced states in conventional and unconventional superconductors. *Rev. Mod. Phys.* **78**, 373–433 (2006). doi:10.1103/RevModPhys.78.373
42. M. Bode, M. Getzlaff, R. Wiesendanger, Spin-polarized vacuum tunneling into the exchange-split surface state of Gd(0001). *Phys. Rev. Lett.* **81**, 4256–4259 (1998). doi:10.1103/PhysRevLett.81.4256
43. O. Pietzsch, A. Kubetzka, M. Bode, R. Wiesendanger, Spin-polarized scanning tunneling spectroscopy of nanoscale cobalt islands on Cu(111). *Phys. Rev. Lett.* **92**, 057202 (2004). Medline doi:10.1103/PhysRevLett.92.057202
44. J. Moser, A. Matos-Abiague, D. Schuh, W. Wegscheider, J. Fabian, D. Weiss, Tunneling anisotropic magnetoresistance and spin-orbit coupling in Fe/GaAs/Au tunnel junctions. *Phys. Rev. Lett.* **99**, 056601 (2007). Medline doi:10.1103/PhysRevLett.99.056601
45. K. T. Law, P. A. Lee, T. K. Ng, Majorana fermion induced resonant Andreev reflection. *Phys. Rev. Lett.* **103**, 237001 (2009). Medline doi:10.1103/PhysRevLett.103.237001
46. A. A. Zyuzin, D. Rainis, J. Klinovaja, D. Loss, Correlations between Majorana fermions through a superconductor. *Phys. Rev. Lett.* **111**, 056802 (2013). Medline doi:10.1103/PhysRevLett.111.056802
47. C. Fang, M. J. Gilbert, B. A. Bernevig, New class of topological superconductors protected by magnetic group symmetries. *Phys. Rev. Lett.* **112**, 106401 (2014). Medline doi:10.1103/PhysRevLett.112.106401
48. B. B. Zhou, S. Misra, E. H. da Silva Neto, P. Aynajian, R. E. Baumbach, J. D. Thompson, E. D. Bauer, A. Yazdani, Visualizing nodal heavy fermion superconductivity in $CeCoIn_5$. *Nat. Phys.* **9**, 474–479 (2013). doi:10.1038/nphys2672
49. A. I. Larkin, Y. N. Ovchinnikov, *Sov. Phys. JETP* **20**, 762 (1965).
50. P. Fulde, R. A. Ferrell, Superconductivity in a strong spin-exchange field. *Phys. Rev.* **135**, A550–A563 (1964). doi:10.1103/PhysRev.135.A550
51. J. Li, T. Neupert, B. A. Bernevig, A. Yazdani, *arXiv:1404.4058 [cond-mat]*, (2014).
52. W. Zhong, G. Overney, D. Tománek, Structural properties of Fe crystals. *Phys. Rev. B* **47**, 95–99 (1993). doi:10.1103/PhysRevB.47.95
53. J. C. Budich, E. Ardonne, Equivalent topological invariants for one-dimensional Majorana wires in symmetry class D. *Phys. Rev. B* **88**, 075419 (2013). doi:10.1103/PhysRevB.88.075419
54. G. Kresse, J. Hafner, Ab initio molecular dynamics for liquid metals. *Phys. Rev. B* **47**, 558–561 (1993). doi:10.1103/PhysRevB.47.558
55. G. Kresse, J. Furthmüller, Efficient iterative schemes for ab initio total-energy calculations using a plane-wave basis set. *Phys. Rev. B* **54**, 11169–11186 (1996). doi:10.1103/PhysRevB.54.11169
56. H. J. Monkhorst, J. D. Pack, Special points for Brillouin-zone integrations. *Phys. Rev. B* **13**, 5188–5192 (1976). doi:10.1103/PhysRevB.13.5188
57. K. Würde, A. Mazur, J. Pollmann, Surface electronic structure of Pb(001), Pb(110), and Pb(111). *Phys. Rev. B* **49**, 7679–7686 (1994). doi:10.1103/PhysRevB.49.7679
58. M. P. L. Sancho, J. M. L. Sancho, J. M. L. Sancho, J. Rubio, Highly convergent schemes for the calculation of bulk and surface Green functions. *J. Phys. F Met. Phys.* **15**, 851–858 (1985). doi:10.1088/0305-4608/15/4/009
59. K. J. Franke, G. Schulze, J. I. Pascual, Competition of superconducting phenomena and Kondo screening at the nanoscale. *Science* **332**, 940–944 (2011). Medline doi:10.1126/science.1202204

Acknowledgments: We thank F. von Oppen, L. Glazman, D. Loss, A. Stern, J. Alicea, M. Franz, R. Lutchyn, C-K. Shih, B. Feldman, M. Randeria, P. Lee, and N. P. Ong, for helpful discussions. The work at Princeton has been primarily supported by Majorana Basic Research Challenge grant through ONR-N00014-14-1-0330, ONR-N00014-11-1-0635, ONR- N00014-13-10661, NSF-MRSEC programs through the Princeton Center for Complex Materials DMR-0819860, and NSF CAREER DMR-095242. Work at UT Austin was supported by ONR-N00014-14-1-0330 and by the Welch Foundation grant TBF1473. This project was also made possible using the facilities at Princeton Nanoscale Microscopy Laboratory supported by grants through NSF-DMR-1104612, ARO-W911NF-1-0262, ARO-MURI program W911NF-12-1-0461, DOE-BES, DARPA-SPWAR Meso program N6601-11-1-4110, LPS and ARO-W911NF-1-0606, and the W. Keck Foundation. AY, AB, and Princeton University have filled a provisional patent related to this work. S. N-P acknowledges support of the EU Marie Curie program (IOF 302937). JL acknowledges support of Swiss National Science Foundation. AY acknowledges the hospitality of the Aspen Center for Physics, supported under NSF Grant No. PHYS-1066293.

Supplementary Materials

www.sciencemag.org/cgi/content/full/science.1259327/DC1
Materials and Methods
Supplementary Text
Figs. S1 to S16
Table S1
References (*52*–*59*)

28 July 2014; accepted 19 September 2014
Published online 2 October 2014
10.1126/science.1259327

Downloaded from http://science.sciencemag.org/ on October 25, 2017

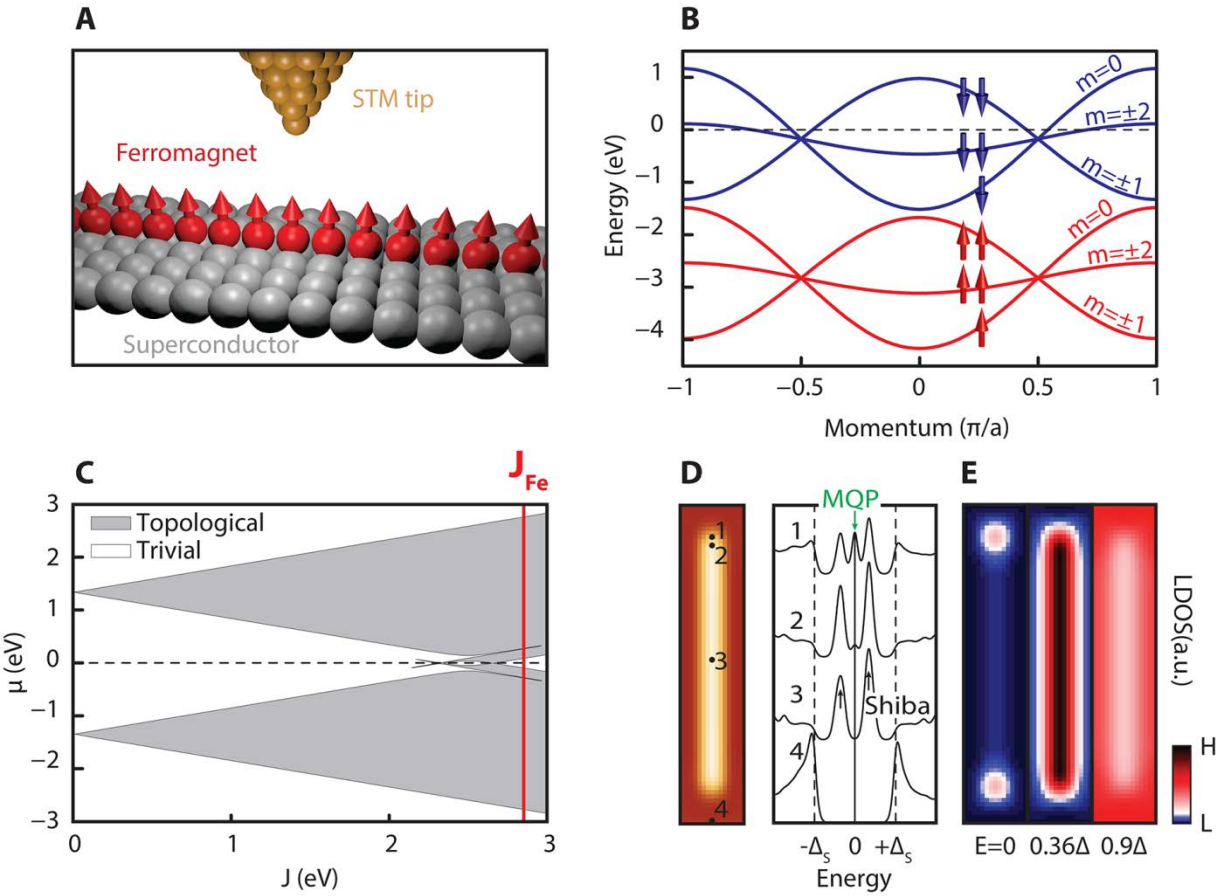


Fig. 1. Topological superconductivity and Majorana fermions in Ferromagnetic atomic chains on a superconductor. (**A**) Schematic of the proposal for Majorana quasi-particle (MQP) realization and detection: a ferromagnetic atomic chain is placed on the surface of strongly spin-orbit (SO) coupled superconductor and studied using scanning tunneling microscopy (STM). (**B**) Band structure of a linear suspended Fe chain before introducing spin-orbit coupling or superconductivity. The majority spin-up (red) and minority spin-down (blue) d-bands labeled by azimuthal angular momentum m are split by the exchange interaction *J* (degeneracy each band is noted by the number of arrows). (**C**) Regimes for trivial and topological superconducting phases are identified for the band structure shown in (B) as a function of exchange interaction in presence of SO coupling. The value *J* for Fe chains based on DFT calculations is noted [sections 1 and 3 of (*36*)]. (**D**) Model calculation of the local density of states (LDOS) of the atomic chain embedded in a 2D superconductor [section 2 of (*36*)]. Left panel shows an image of the chain and the locations at which the LDOS is represented in the right panel; the LDOS curves are offset for clarity. In-gap (Shiba) and zero-energy (MQP) features in LDOS are noted. (**E**) Spatially resolved LDOS calculated at various energies noted at the bottom using the same model. Red (blue) indicates regions of the high (low) LDOS.

Downloaded from http://science.sciencemag.org/ on October 25, 2017

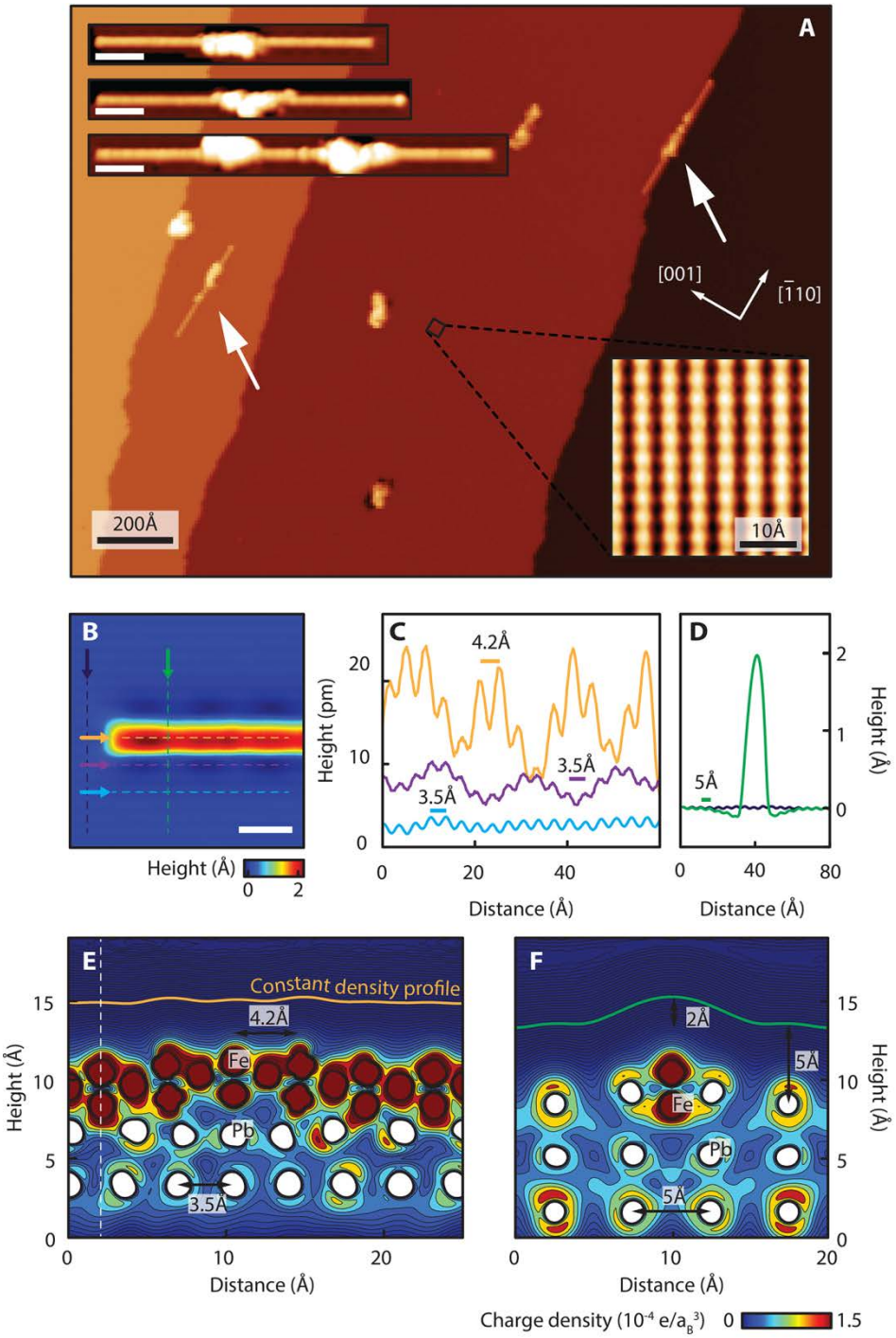


Fig. 2. Atomic Fe chains on Pb (110). (**A**) Topograph of the Pb (110) surface after growth of Fe showing Fe islands and chains indicated by white arrows and atomically clean terraces of Pb (regions with the same color) with size exceeding 1000 Å. Lower-right inset shows the anisotropic atomic structure of the Pb(110) surface with interatomic distances in the two directions, *a* = 4.95 Å and $a/\sqrt{2} = 3.5$ Å, as expected for the face-centered cubic crystal structure. Upper-left insets show images of several atomic Fe chains and islands from which they grow (scale bar corresponds to 50 Å). (**B**) Fine scale topograph. The color-coded lines correspond to the line traces in (C) and (D). The scale bar corresponds to 20 Å. (**C**) A cross section of the image in (B) along the chain measured on top of the chain (light brown) and along two different lines next to the chains (purple and blue) showing atomic corrugation of the chain and strain induced in the substrates. Both are influenced by the incommensurate placement of the Fe atoms in Pb. (**D**) Apparent STM height profile on the substrate (black) and across the atomic chain (green). (**E** and **F**) Atomic structure of the zigzag chain as calculated using DFT [section 3 of (*36*)] along (A) and across (F) the chain. The Fe chain structure that has the lowest energy in the DFT calculations matches the structural features in the STM measurements (B to D). All measurements were carried out at 1.4 K.

Downloaded from http://science.sciencemag.org/ on October 25, 2017

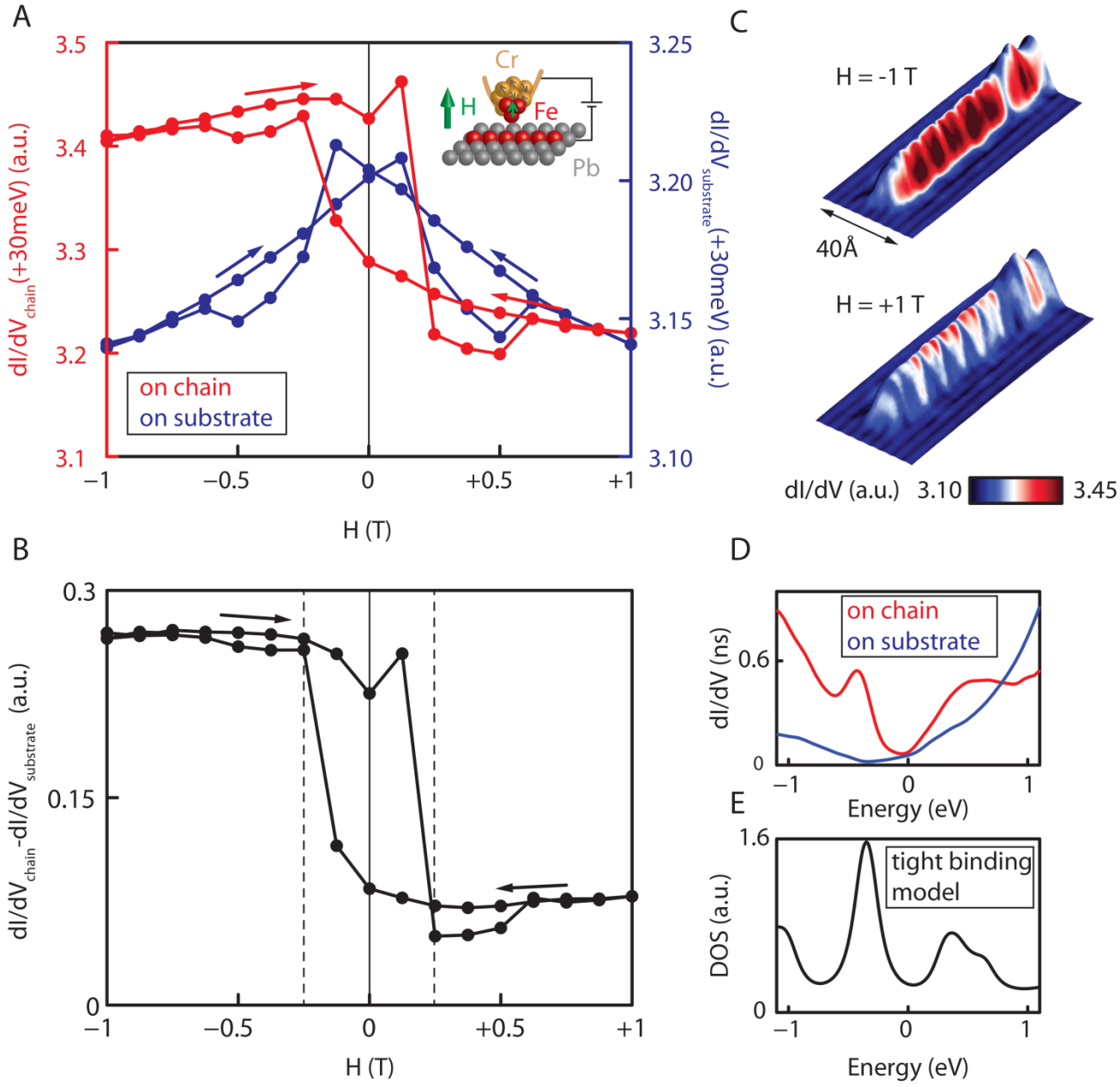


Fig. 3. Spin-polarized measurements and normal state characterization of Ferromagnetic chains. (**A**) Spatially average (over region of about 100 Å) STM tunneling conductance as a function out-of-plane applied magnetic field H on the atomic chain and the substrate measured with a spin-polarized bulk Cr/Fe tip (inset shows a schematic of the measurement, set point V = 30 mV, I = 0.75 nA). Tip switching occurs at ± 0.25 T. (**B**) Difference between conductance on and off the chain shown in (A). (**C**) Topography of the chain colorized by the conductance at ±1 T from low conductance (dark blue) to high conductance (dark red). (**D**) STM point spectra of the atomic chain and the substrate. (**E**) DOS computed using tight binding model of a zigzag Fe chain as describe in section 4 of (*36*).

Downloaded from http://science.sciencemag.org/ on October 25, 2017

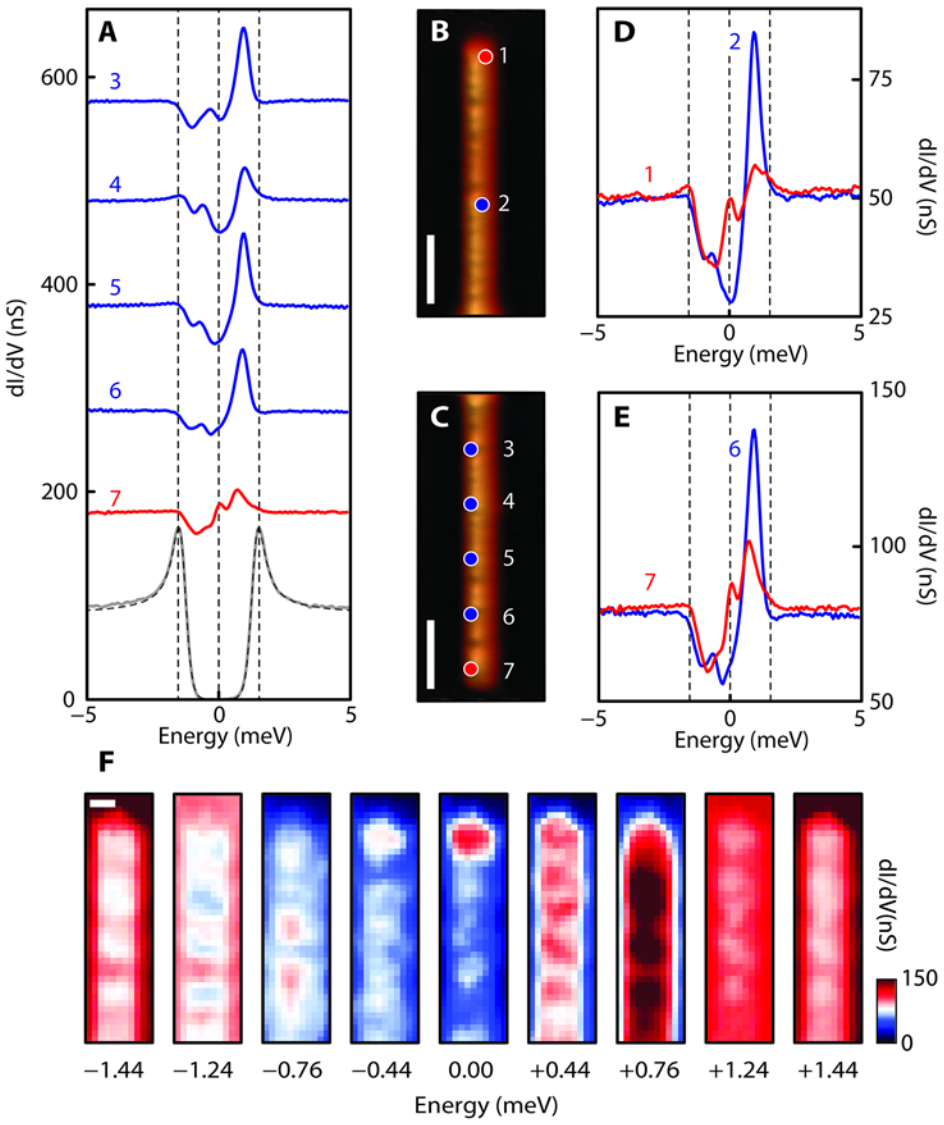


Fig. 4. Spectroscopic mapping of atomic chains and ZBPs. (**A**) STM spectra measured on the atomic chain at locations corresponding to those indicated in panels (B) and (C). For clarity, the spectra are offset by 100 nS. The red spectrum shows the ZBP at one end of the chain. The gray trace measured on the Pb substrate can be fit using thermally broadened BCS DOS (dashed gray line, fit parameters Δ_s = 1.36 meV, T = 1.45 K). (**B** and **C**) Zoom-in topography of the upper end (B) and lower end (C) of the chain and corresponding locations for spectra marked (1-7). (**D** and **E**) Spectra measured at marked location as in (B) and (C). (**F**) Spatial and energy-resolved conductance maps of another Fe atomic chain close to its end, which shows similar features in point spectra as in (A). Conductance map at zero bias (middle panel) shows increased conductance close to the end of the chain. Scale bar corresponds to 10 Å. We note that the localization length of the MQP observed here is a factor of 10 or smaller in length than the distance from the end to the islands that form in the middle of the chains.

Downloaded from http://science.sciencemag.org/ on October 25, 2017

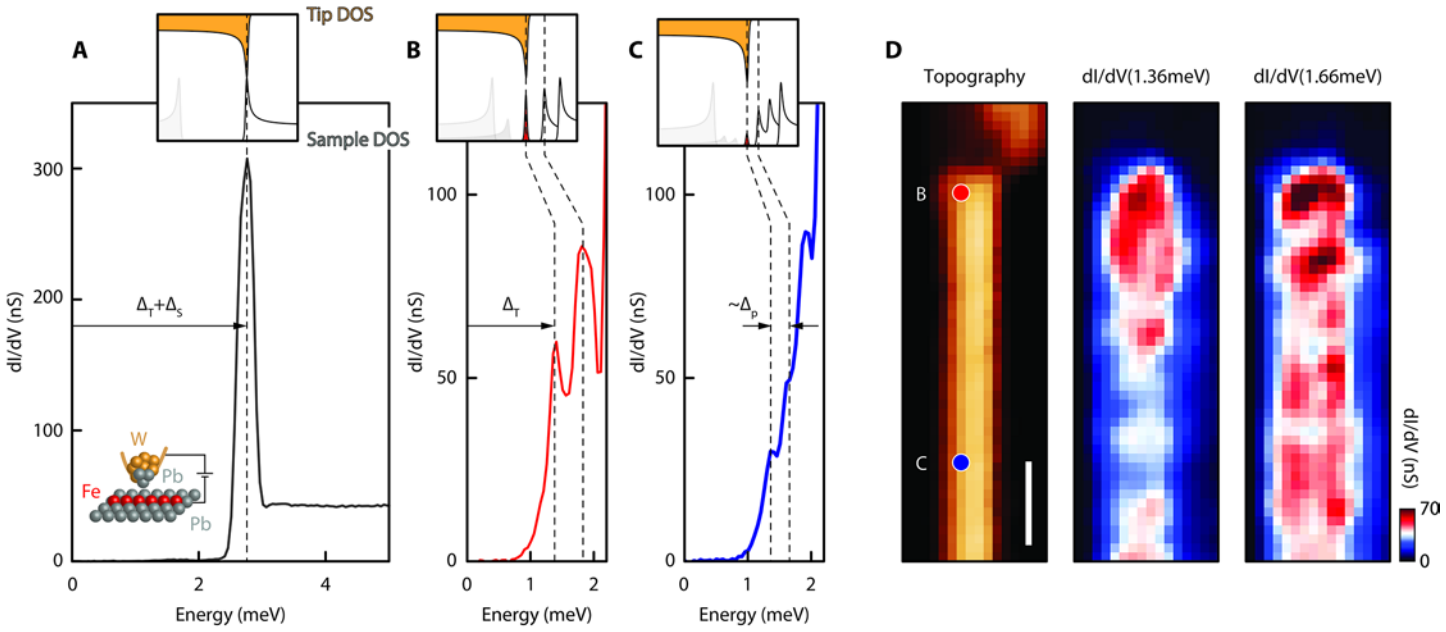


Fig. 5. High energy-resolution spectra obtained using a superconducting tip. (**A**) Point spectra on the superconducting substrate (with a gap of Δ_S) using the superconducting tip (with a gap of Δ_T) shows a peak at $\Delta_T + \Delta_S$. Upper schematic shows alignment of the BCS DOS for the tip and the sample as a function of bias, which results in the conductance at $\Delta_T + \Delta_S$ and suppressed conductance at lower voltages. (**B**) STM spectra at the end of the Fe chain showing a peak at Δ_T which corresponds to the ZBP (inset shows schematics of the DOS alignment between the tip and the sample). The shape of the spectra and the higher peak indicate that the ZBP resides in a gap even at the end of the wire. (**C**) Point spectra in the middle of the Fe atomic chain showing a peak at Δ_T + 300 μV, signaling the approximate value of the effective p-wave gap in the bulk of the chain. (**D**) Topographic image of the atomic chain and spatially resolved conductance maps for $|eV_1| = \Delta_T = 1.36$ meV and $|eV_2| = \Delta_T + 0.3$ meV. The left image indicates where the point spectra in panels (B) and (C) are taken. The scale bar corresponds to 20 Å.

Downloaded from http://science.sciencemag.org/ on October 25, 2017

Science

Observation of Majorana fermions in ferromagnetic atomic chains on a superconductor

Stevan Nadj-Perge, Ilya K. Drozdov, Jian Li, Hua Chen, Sangjun Jeon, Jungpil Seo, Allan H. MacDonald, B. Andrei Bernevig and Ali Yazdani

published online October 2, 2014

ARTICLE TOOLS http://science.sciencemag.org/content/early/2014/10/01/science.1259327

SUPPLEMENTARY MATERIALS http://science.sciencemag.org/content/suppl/2014/10/01/science.1259327.DC1

RELATED CONTENT http://science.sciencemag.org/content/sci/346/6209/545.full

REFERENCES This article cites 56 articles, 3 of which you can access for free
http://science.sciencemag.org/content/early/2014/10/01/science.1259327#BIBL

PERMISSIONS http://www.sciencemag.org/help/reprints-and-permissions

Use of this article is subject to the Terms of Service

Science (print ISSN 0036-8075; online ISSN 1095-9203) is published by the American Association for the Advancement of Science, 1200 New York Avenue NW, Washington, DC 20005. 2017 © The Authors, some rights reserved; exclusive licensee American Association for the Advancement of Science. No claim to original U.S. Government Works. The title *Science* is a registered trademark of AAAS.

Downloaded from http://science.sciencemag.org/ on October 25, 2017